Figure S1. Scheme of sputtering chamber
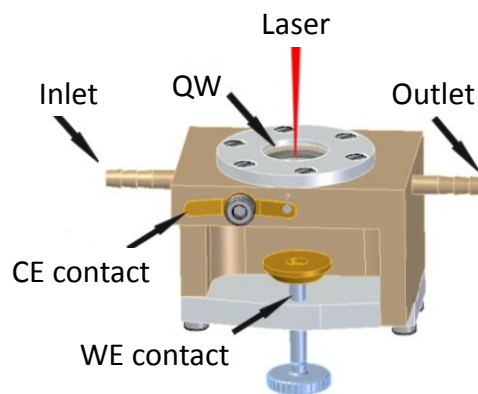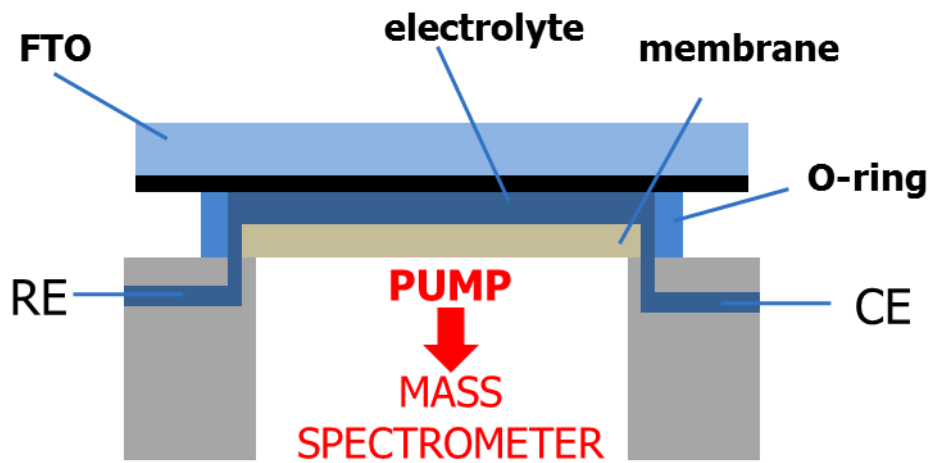

Figure S2. Scheme of an electrochemical cell coupled with a Raman spectrometer for in-situ measurements.
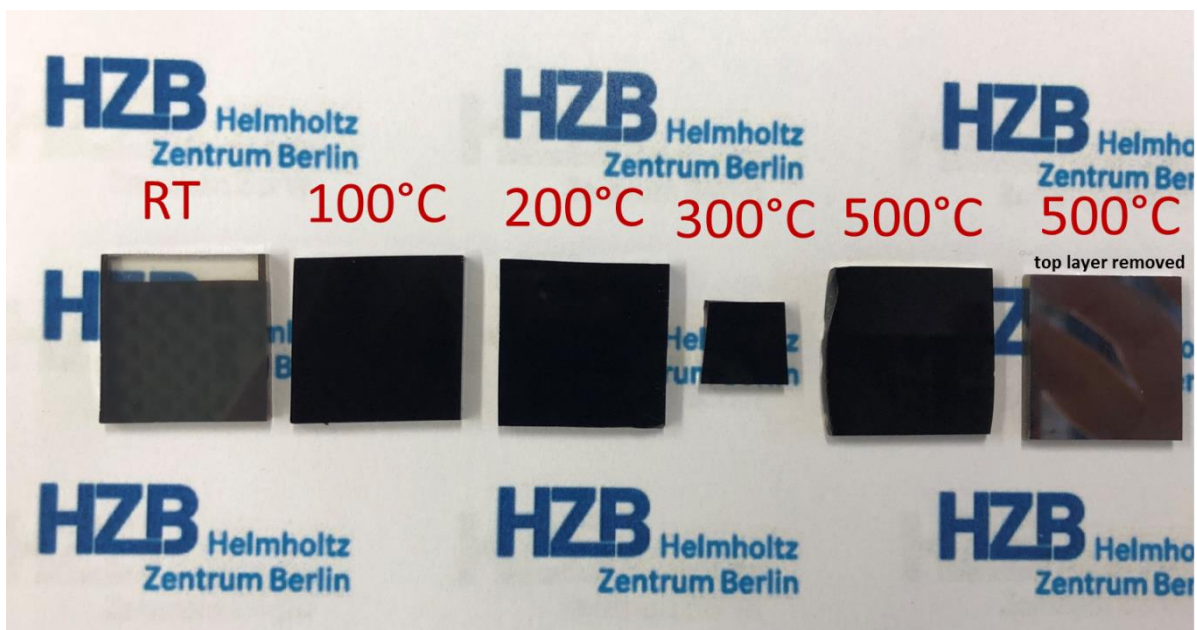
Figure S3. Scheme of the DEMS cell

Figure S4. Photos of molybdenum sulfide electrodes sputtered at different temperatures. For films grown at higher temperatures, the top part of the film consists of a porous layer while the bottom part is a more compact film. For the right-most sample in this series of photographs, the porous top layer is removed, revealing the shiny layer underneath.
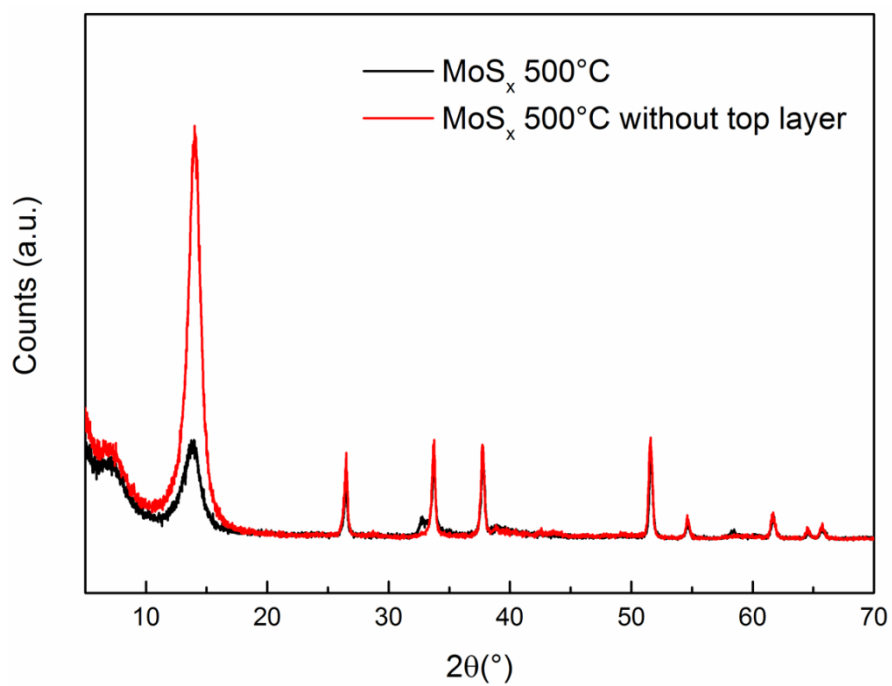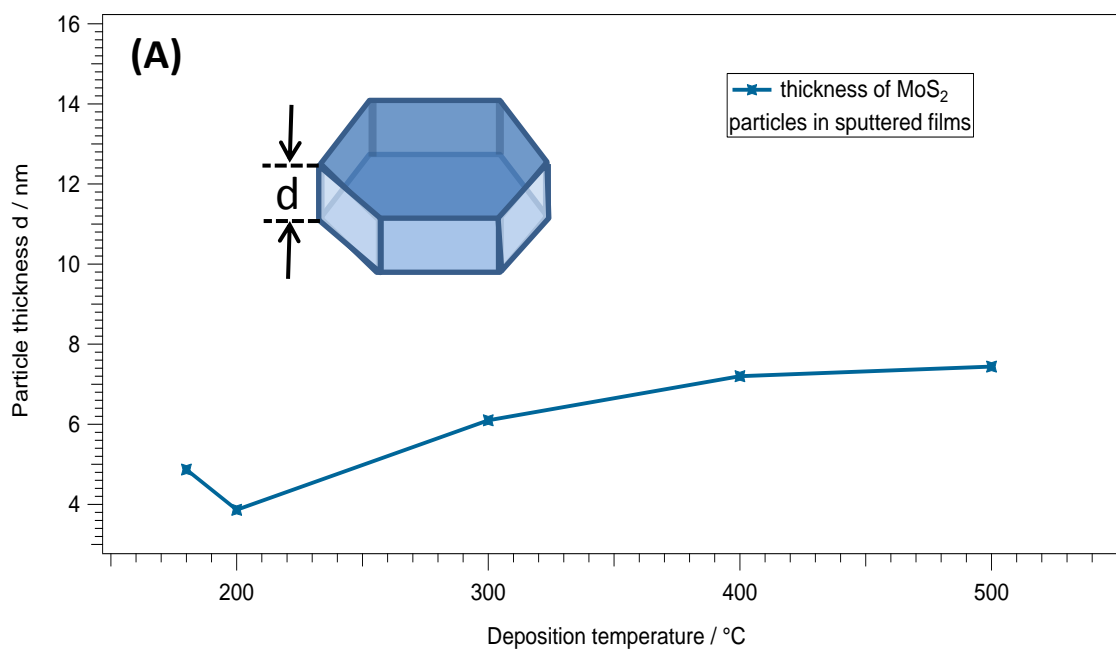
Figure S5. XRD patterns of a MoS$_x$ sputtered at 500 °C as grown (black curve) and after removal of the porous layer on top.
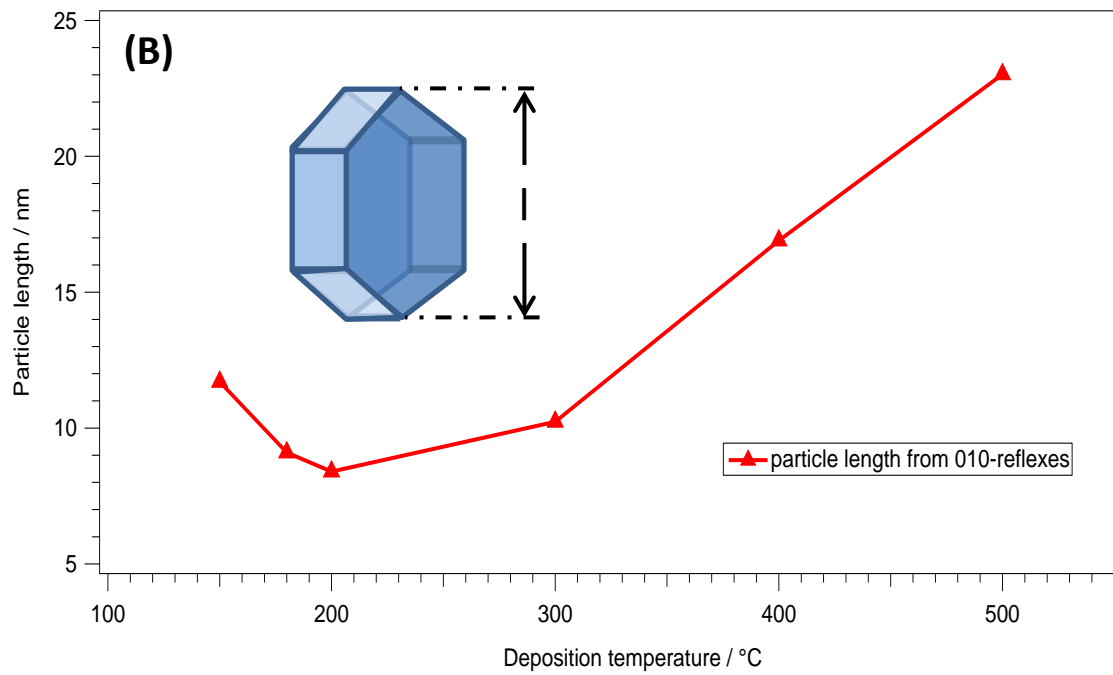
Figure S6. (A) Mean thickness of (00.1) oriented hexagonal platelets in the MoS$_2$ layers determined from FWHM values of X-ray diffractograms as shown in Fig. 2.A determined from Scherrer´s equation; (B) Mean length l of (01.0) oriented hexagonal platelets in the layers determined from FWHM values of X-ray diffractograms shown in Fig. 2.A using Scherrer´s equation.
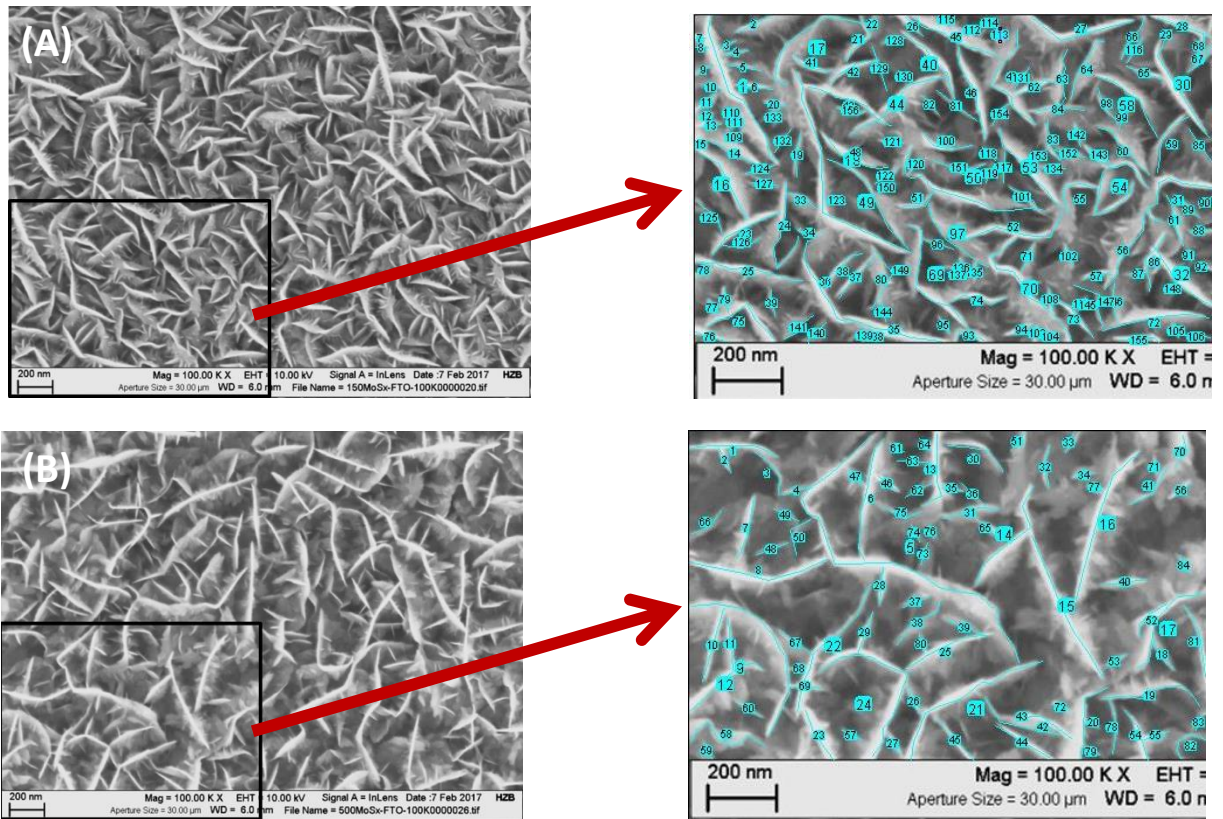
Figure S7. Estimation of the edge lengths of (hk.0) facets per area in MoS$_x$ films prepared at 150°C (A) and 500°C (B).
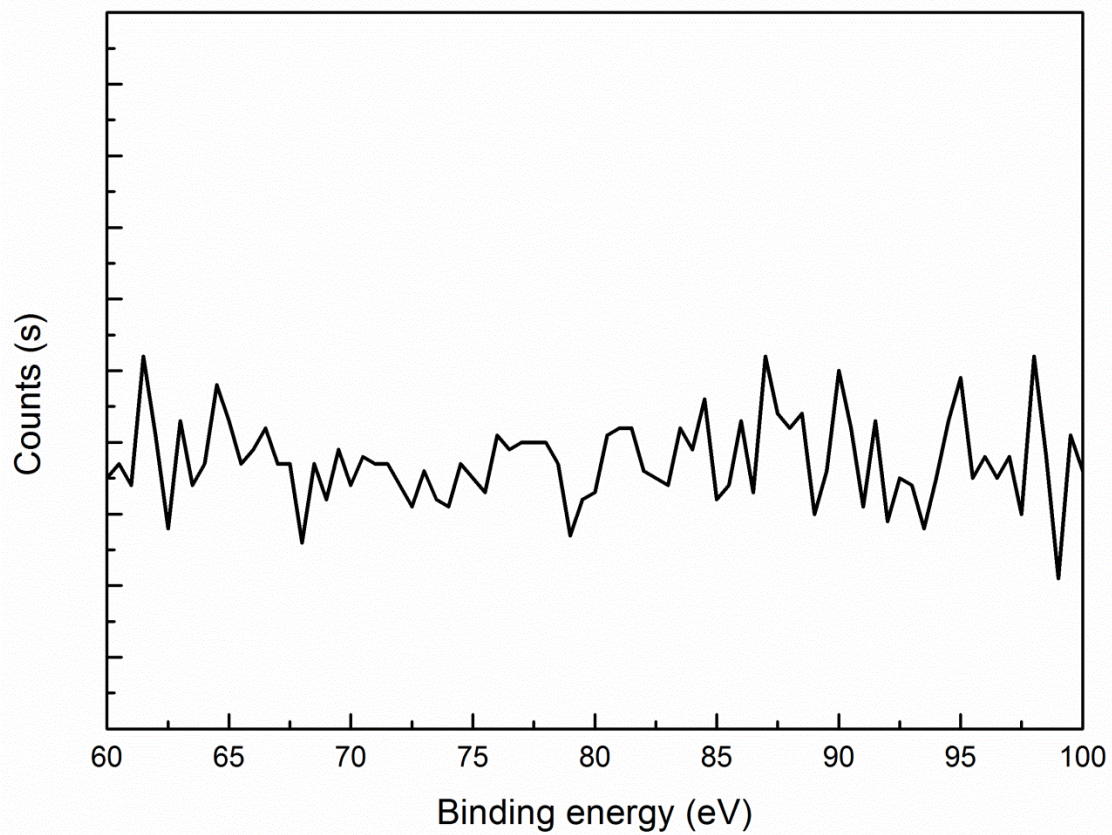
Figure S8. XPS spectrum at the region of Pt 4f of MoS$_x$ tested for 2h cycling from 0.2V to -0.3V vs RHE.
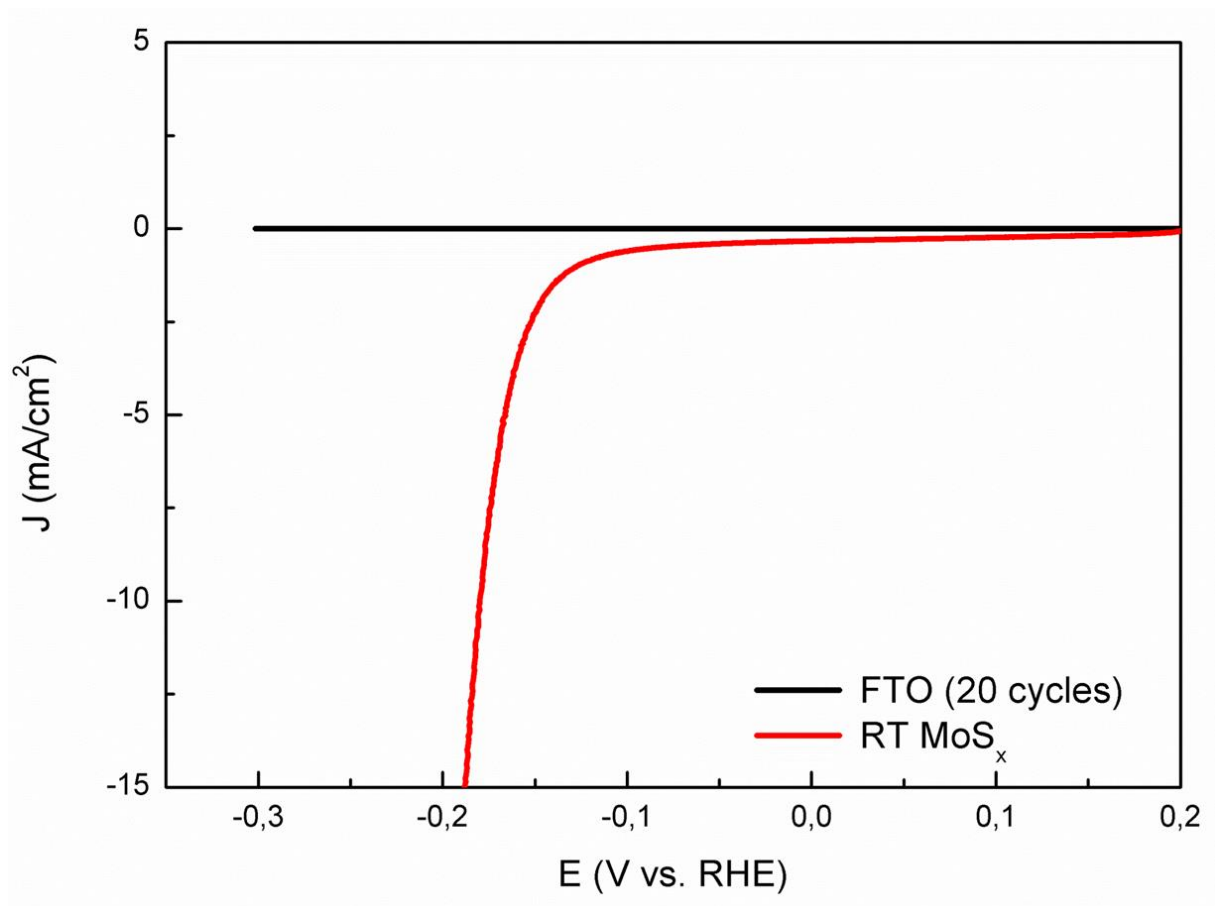
Figure S9. CV of FTO substrate for 20 cycles (33min) compared with CV of room temperature sputtered MoS$_x$
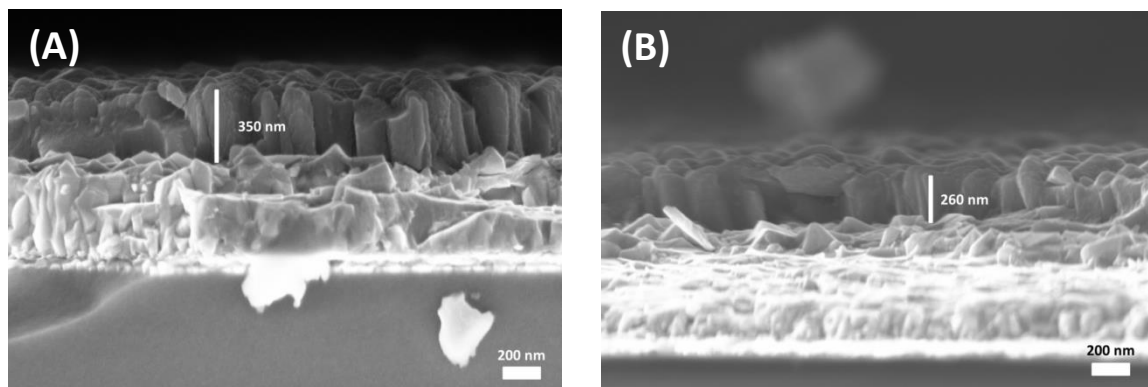
Figure S10. (A) cross section SEM of as-prepared MoS$_x$; (B) cross section SEM of MoS$_x$ electrode after 10min. electrochemical cycling.

Figure S11. Top view morphology of MoS$_x$ electrode after 2h electrochemical measurement.

Figure S12. Raman spectra of RT MoS$_x$ measured in an in-situ electrochemical cell using 0.5 M H$_2$SO$_4$ electrolyte before and after CV cycling.

8

Figure S13. Raman spectra of RT sputtered MoS$_x$ after electrochemical cycling: original (red) and blue (exposed in air)

Supplementary Note 1: DFT calculations on [Mo$_3$S$_{13}$]$^{2-}$ ligand

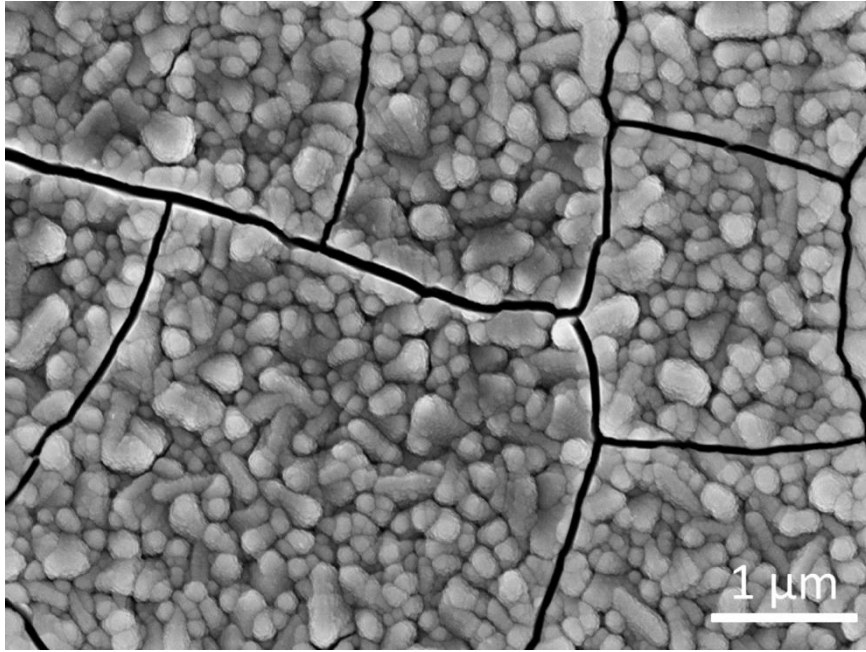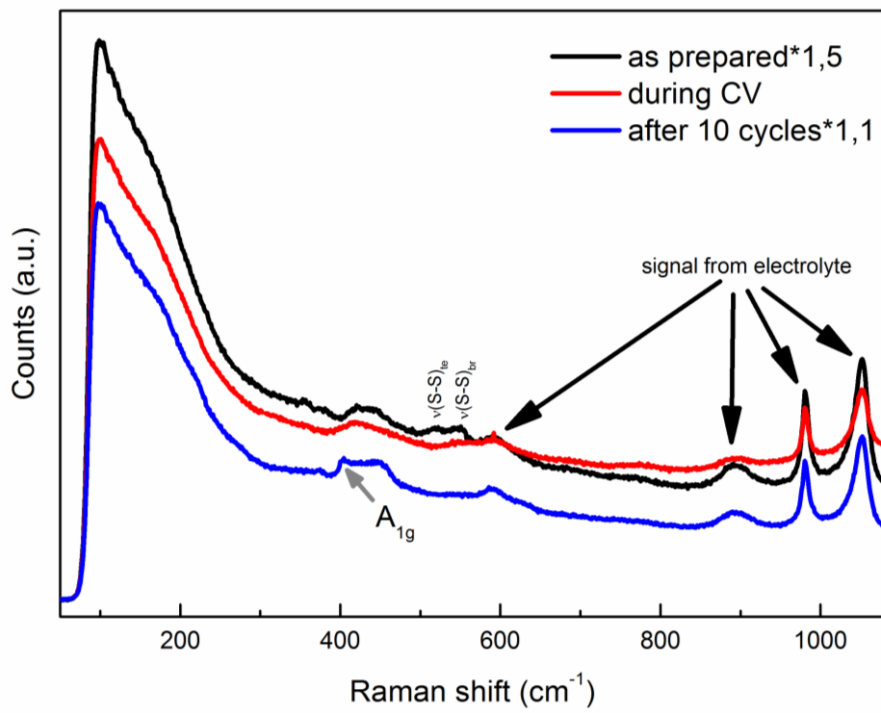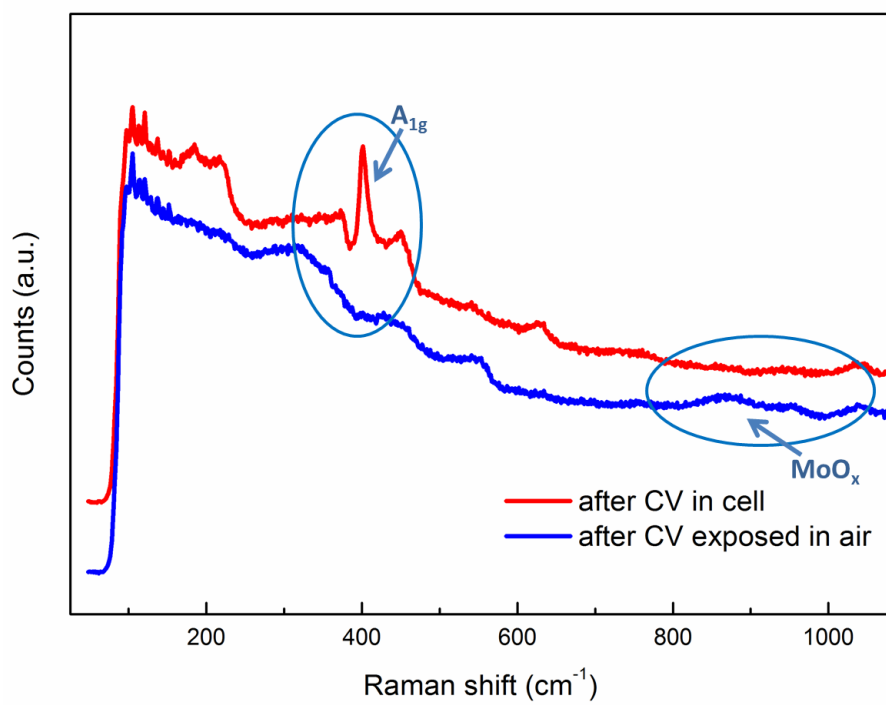As shown in Figure S14 (B), the cluster Mo$_3$S$_{13}$ shows a similar structure to the edge of monolayer MoS$_2$. The highest occupied molecular orbital (HOMO) and lowest unoccupied molecular orbital (LUMO) has shown in Figures S14 (A) and (B), respectively. The HOMO is mainly located at the S atoms that solely bond to one Mo atom, denoted as terminal S (S$_t$), while the LUMO is centred in the S atoms that shared by two Mo atoms, denoted as bridging S (S$_b$). The one shared by three Mo atoms located in the centre is denoted as S$_a$. According to the HER reaction equation, listed below, the reaction site should be more favourable at those solely S$_t$ atoms.
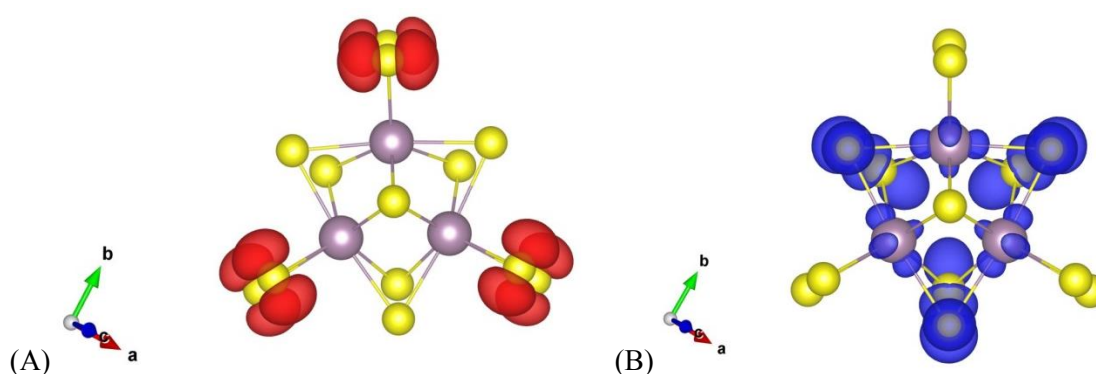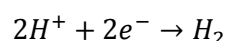
$$2H^+ + 2e^- \rightarrow H_2$$

(A)　　　　　　　　　　　　　　　　　　　　(B)

Figure S14. The HOMO (A) and LUMO (B) of Mo$_3$S$_{13}$ cluster. Isosurface= 0.005e/a$_0$^{3}, where a$_0$ is Bohr radii.

This conclusion is also confirmed in the calculated H* DFT binding energies, using the following equation;

$$E_{ad} = E_{total} - E_{cluster+H} - \frac{1}{2}E_{H_2}$$

where the $E_{cluster+H}$ represents that cluster with the number of H adsorption. And E_{H2} is the energy of H$_2$ molecule. Five different sites were considered, denoted as c, t_up, t_down, b_up and b_down, which represents bonding to S$_a$, up S$_t$, lower S$_t$, up S$_b$ and lower S$_b$, respectively. Here we define the up and lower S by whether it is located on the same side as S$_a$ or not.

The Gibbs free energy of the intermedia were obtained by $\Delta G_H^0 = E_{ad} - T\Delta S + \Delta ZPE$, where T is the temperature, ΔS is the entropy change of adsorption of H, and ΔZPE is the zero-point energy. As shown in Figure S15, the Mo$_3$S$_{13}$ possessed excellent HER catalysis, due to the terminal S. Whereas, the bridging S require relatively high overpotentials.

Table S1. The binding energy (eV) and bonds length (Å) of first H* on five different sites of Mo$_3$S$_{13}$ cluster.

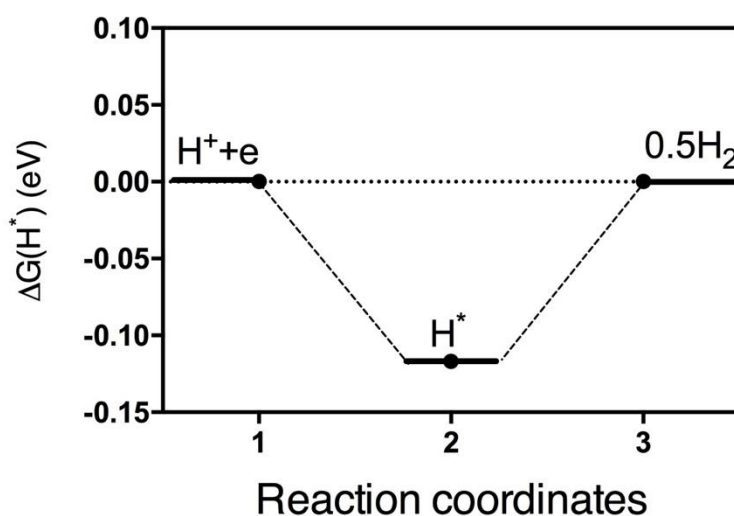|	E$_{ad}$ (eV)	ΔG_{H*}^0 (eV)_	bond length (Å)
a	0.895	1.13	1.364
t_up	-0.36	-0.117	1.369
t_lower	-0.45	-0.209	1.368
b_up	1.678	1.92	1.383
b_lower	1.567	1.80	1.410

Figure S15. Calculated free energy of the reaction intermediate (in eV).

Calculation details

All DFT calculations were performed using the Vienna *ab-initio* Package (VASP).[i] The projected augmented wave (PAW) potentials are adopted to treat the core electrons and electron exchange and correlation were treated using by PBE functional.[ii] As previous benchmarking calculations suggested, the semi core *p* states of Mo was treated as valence.[iii] The energy cutoff was set to 350 eV, which is 35% higher than the default one. All the atoms are fully relaxed until the total energies are converged up to 10^{-5} eV and the Hellmann-Feynman forces are less than 0.01 eV /Å. For the H* adsorption on cluster, van der Waals corrections was adopted DFT-D2 method of Grimme.[iv]

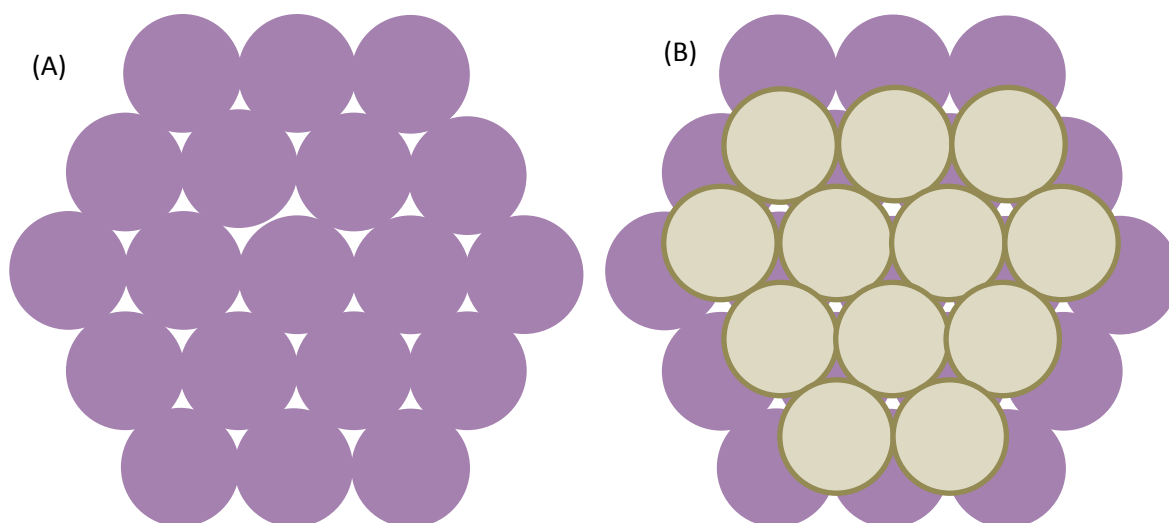**Supplementary Note 2: Calculation of MoS$_2$ particle size**

Figure S16. (A) Scheme of a close packed Mo layer and (B) of a Mo layer sandwiched by two S layers in hexagonal MoS$_2$ nano-particles.

In this calculation, one assumption has to be made the molybdenum layer has the shape of regular hexagon and the number of Mo atoms on one edge is n, therefore

the number of Mo atoms on the edge is

$$N_e = 6n-6$$

And the overall number of Mo atoms is

$$N_{all} = 3n^2-3n+1$$

The number of inside Mo atoms is

$$N_{in} = N_{all} - N_e = 3n^2-9n+7$$

As we can see from Fig. S16 (B), the number of sulfur atoms in MoS_2 particles should be

$$N_S = 2*(N_{all}-3*n+2) = 6n^2-12n+6$$

In our hypothesis, only the Mo atoms on the edge will be oxidized after taken out from electrolyte, therefor the ratio of Mo(6+) to Mo(4+) in the partially oxidized sample

$$Mo(6+) : Mo(4+) = N_e/N_{in}$$

From XPS results, it is known that after 10min of cycling, the ratio of Mo(6+) : Mo(4+) is 1 : 4.56, then the n value we calculated is around 11 which means there are about 331 Mo atoms and 600 S atoms in the particle.

After 2h of cycling, the Mo(6+) : Mo(4+) of 1 : 3.14, then the value of n should be around 8, and the particle consists of about 169 Mo atoms, 294 S atoms.

[i] G. Kresse, and J Furthmüller, *Phys. Rev. B*, **54**, 11169, 1996

[ii] J. P. Perdew, J. A. Chevary, S. H. Vosko, K. A. Jackson, M. R. Pederson, D. J. Singh, and C. Fiolhais, *Phys. Rev. B*, **46**, 6671, 1992

[iii] A. Jain, G. Hautier, C. J. Moore, S. P. Ong, C. C. Fischer, T. Mueller, K. A. Persson, and G. Ceder, *Comput. Mater. Sci.*, **50**, 2295, 2011

[iv] S. Grimme, *J. Comp. Chem.*, **27**, 1787, 2006